



Development of a pyrolysis model for oriented strand board. Part I: Kinetics and thermodynamics of the thermal decomposition

Journal of Fire Sciences

2021, Vol. 39(2) 190–204

© The Author(s) 2021

Article reuse guidelines:

sagepub.com/journals-permissions

DOI: 10.1177/0734904120982887

journals.sagepub.com/home/jfs

Junhui Gong^{1,2} , Hong Zhu^{1,3}, Hongen Zhou¹ and Stanislav I Stoliarov¹

Date received: 24 August 2020; accepted: 3 December 2020

Abstract

Oriented strand board is a widely used construction material responsible for a substantial portion of the fire load of many buildings. To accurately model the response of oriented strand board to fire, thermogravimetric analysis, differential scanning calorimetry, and microscale combustion calorimetry tests were carried out to construct a thermal decomposition model using a numerical solver, ThermaKin, and a hill climbing optimization algorithm. The model included a single-step water vaporization reaction and four consecutive reactions representing thermal decomposition of organic constituents of oriented strand board. The experiments and modeling revealed that the first two of the four reactions are endothermic, while the last two are exothermic. The net heat of decomposition was found to be near zero. The heat capacities of condensed-phase species and heats of combustion of evolved gases were also determined. The heats of combustion were found to vary over the course of decomposition—the trend captured by the model. Development of a complete pyrolysis model for this material will be a subject of Part II of this work.

Keywords

Oriented strand board, thermal analysis, decomposition reactions, heat of decomposition, heat of combustion, ThermaKin

¹Department of Fire Protection Engineering, University of Maryland, College Park, MD, USA

²College of Safety Science and Engineering, Nanjing Tech University, Nanjing, China

³State Key Laboratory of Fire Science, University of Science and Technology of China, Hefei, China

Corresponding author:

Junhui Gong, College of Safety Science and Engineering, Nanjing Tech University, Puzhu Road 30, Pukou District, Nanjing 210009, China.

Email: gjh9896@njtech.edu.cn

Introduction

Oriented strand board (OSB) is a type of engineered wood formed by coating wood strands with a small amount of adhesive (wax or resin) and then compressing layers of wood strands in specific orientations into panels. OSB is extensively utilized in construction for load-bearing as well as non-load-bearing applications due to its favorable mechanical properties and low cost. Exterior and internal wall construction is perhaps the most common application of OSB. OSB is more widely used than plywood and particle board, commanding 66% of the structural panel market.¹ OSB composition and performance is a subject of a number of mechanical performance standards including PS2-10 in the United States, EN 300 in Europe, CAN/CSA O325 and CSA O437 in Canada, and GB/T 4897-2015 in China. One of the main disadvantages associated with utilization of OSB in built environment is its inherent flammability related to carbon-based nature of this material. To design adequate fire protection, it is important to be able to determine how much OSB contributes to fire growth in a given scenario. Determination of this contribution relies on the knowledge of a set of properties that define the response of a solid material to external heat and referred to as pyrolysis properties.

Pyrolysis of a combustible solid can be relatively well described by a set of semi-global reactions and relevant kinetic and energetic parameters. The kinetic parameters are typically obtained from thermogravimetric analysis (TGA) tests interpreted using analytical or numerical methods. Inverse modeling and heuristic algorithms, such as genetic algorithm (GA), particle swarm optimization (PSO), and multi-objective optimization, are frequently employed to determine the kinetic parameters. The kinetics of thermal decomposition of various forms of biomass have been derived using GA,²⁻⁴ and PSO^{5,6} algorithms. Ding et al.⁷ compared the accuracy and efficiency of the two approaches using a three-component parallel reaction mechanism obtained for beech wood and found that PSO showed a better performance. Richter and Rein estimated the chemical kinetics for microscale pyrolysis of cellulose,⁸ timber,⁹ softwood, and hardwood^{10,11} using a multi-objective optimization algorithm. The derived kinetic parameters yielded reasonable predictions of the literature data collected in air as well as inert environment.

Thermodynamic parameters, including heats of individual decomposition steps and heat capacities of the condensed-phase reactants and products, have also been shown to be important for accurate pyrolysis modeling.¹² Li and Stoliarov^{13,14} first demonstrated how these properties can be derived from differential scanning calorimetry (DSC) experiments that were conducted simultaneously with TGA tests. McKinnon and Stoliarov^{15,16} and Ding et al.¹⁷ extended this analysis by fully accounting for variation in instantaneous heating rate observed in TGA/DSC experiments and including the microscale combustion calorimetry (MCC) testing and inverse modeling to obtain heats of combustion of individual gaseous products defined in multi-step reaction mechanisms. Rinta-Paavola and Hostikka¹⁸ have recently applied a similar methodology to obtain the thermodynamic parameters for spruce and pine.

The pyrolysis and combustion of OSB has been a subject of several prior investigations. Hirle and Balog¹⁹ carried out TGA and bench-scale tests to determine the dependency of auto-ignition time on the applied heat flux. White and Sumathipala²⁰ and Ayrilmis et al.²¹ studied the burning behavior of pure and fire-retarded OSB in a cone calorimeter. Only qualitative analysis of the experimental data was carried out in these studies. Mealy et al.²² performed comprehensive measurements of OSB thermal decomposition, ignitability, and burning and flame spread rates. Some key parameters such as surface ignition temperature and thermal conductivity were derived from these measurements. However, no complete

pyrolysis property set that successfully predicted outcomes of the presented experiments was developed. Most recently, Ira et al.²³ investigated the thermal decomposition of OSB as well as several other engineered wood products. A set of three parallel reactions was used to successfully capture the presented TGA data. A shuffled complex evolution (SCE) optimization algorithm was employed to obtain the kinetic parameters and the initial fraction of each component. However, the decomposition thermodynamics was not determined and the heats of combustion of individual gaseous products were not resolved.

Thus, the purpose of this study was to fill the gaps in knowledge on this important material and develop a model of thermal decomposition that includes heat capacities and heats of reactions and also heats of combustion of gaseous species defined in the mechanism. The model was validated against the TGA data collected at several nominal heating rates. The model was also shown to simultaneously reproduce DSC and MCC data obtained in the current study. A comparison of this model with kinetic models developed by other researches for engineered wood products was also carried out.

Experimental

Material and sample preparation

Several 2.44 m \times 1.22 m \times 0.011 m Georgia-Pacific Blue Ribbon PS2-10-compliant OSB sheets were purchased from a major US distributor. The density of the sheets was measured at room temperature and found to be 664 kg m⁻³, on average. The density was also found to vary significantly, between 550 and 750 kg m⁻³, across the sheet surface and, to a lesser degree, across thickness. The experimental samples were prepared by grinding the sheets into powder. The samples were collected from different parts of the sheets and several grinding techniques were used yielding particles between 20 and 300 μ m in size. Preliminary TGA tests indicated that neither the sample location in the sheet nor grinding technique had any impact on the experimental results. All powders were dried in a desiccator (relative humidity of about 25%) at room temperature for at least 48 h prior to testing to minimize variability in the sample moisture content.

Simultaneous thermal analysis

TGA and DSC tests were conducted simultaneously using a Netzsch 449 F3 Jupiter thermal analyzer, which was calibrated every 3 months following the procedures described in detail in an earlier publication.¹³ The heating program consisted of a conditioning period, where the sample was maintained at 313 K for 25 min, and a linear heating phase with a prescribed heating rate, which stopped when the sample temperature reached 1000 K. All tests were conducted in nitrogen atmosphere to emulate anaerobic conditions of a solid surface covered by a continuous diffusion flame.²⁴ The initial sample mass was between 5 and 7 mg.

Ten tests were performed at a nominal heating rate of 10 K min⁻¹ to accumulate statistics. Both mass and heat flow data were collected in these tests. These tests were performed using Platinum–Rhodium crucibles with lids containing a small opening to maximize the temperature uniformity and heat flow sensitivity, while allowing gaseous pyrolyzate to escape. Three tests were performed at 5 K min⁻¹ and another three tests were performed at 20 K min⁻¹. These six tests were carried out using open ceramic crucibles and only mass data were collected in these tests. The data from these tests were used to determine whether the thermal

decomposition model based on 10 K min^{-1} experiments was able to capture alternate heating scenarios and whether the presence of lids and/or changes in the crucible material had any impact on the mass loss kinetics. Finally, five tests were performed at 10 K min^{-1} on the final decomposition residue or char (collected from several individual tests) to determine heat capacity of this material. These tests were conducted using Platinum–Rhodium crucibles with lids.

MCC testing

The MCC testing of OSB samples was performed in accordance with the corresponding ASTM standard²⁵ in an apparatus calibrated weekly following the recommended protocols.²⁶ The initial mass of the sample was between 4 and 6 mg. The sample was conditioned for 2 min at 348 K and heated with a nominal heating rate of 10 K min^{-1} to 1000 K. Similar to the TGA/DSC tests, the sample was pyrolyzed in nitrogen atmosphere. The gaseous pyrolyzate was mixed with excess oxygen in a high temperature combustor maintained at 1173 K to achieve complete or nearly complete combustion. The oxygen concentration decline in the exhaust gas flow was measured by a calibrated oxygen sensor. The heat release rate (HRR) was subsequently calculated using the oxygen consumption principle²⁶ and recorded as a function of time and pyrolyzing sample temperature. This test was repeated only three times because its results were found to be highly reproducible.

Modeling

A previously developed numerical model, ThermaKin, was employed to simulate TGA/DSC and MCC tests. ThermaKin solves transient energy and species conservation equations formulated as follows

$$\frac{\partial \xi_j}{\partial t} = \sum_{i=1}^{Nr} \theta_i^j r_i - \frac{\partial J_j^x}{\partial x} + \frac{\partial}{\partial x} \left(\xi_j \int_0^x \frac{1}{\rho} \frac{\partial \rho}{\partial t} dx \right) \quad (1)$$

$$\sum_{j=1}^N \xi_j C_{P,j} \frac{\partial T}{\partial t} = \sum_{i=1}^{Nr} h_i r_i - \frac{\partial \dot{q}_x''}{\partial x} - \frac{\partial I_{ex}}{\partial x} + \frac{\partial I_{rr}}{\partial x} - \sum_{g=1}^{Ng} C_{P,g} J_g^x \frac{\partial T}{\partial x} + C_P \rho \frac{\partial T}{\partial x} \int_0^x \frac{1}{\rho} \frac{\partial \rho}{\partial t} dx \quad (2)$$

$$r_i = A_i \exp \left(-\frac{E_i}{RT} \right) \xi_{COMP1} \xi_{COMP2} \quad (3)$$

$$J_g^x = -\rho_g \lambda \frac{\partial}{\partial x} \left(\frac{\xi_g}{\rho_g} \right) \quad (4)$$

$$\dot{q}_x'' = -k \frac{\partial T}{\partial x} \quad (5)$$

$$\frac{\partial I_{ex}}{\partial x} = -I_{ex} \sum_{i=1}^N \kappa_i \xi_i \quad (6)$$

$$\frac{\partial I_{rr}}{\partial x} = \frac{\sigma T^4 \sum_{j=1}^N \epsilon_j v_j}{I_{ex}^0} \frac{\partial I_{ex}}{\partial x} \quad (7)$$

Table 1. Symbols used in the equations (1)–(7).

Symbol (units)	Definition	Symbol (units)	Definition
i	i th reaction	I_{ex} ($W\ m^{-2}$)	Radiant heat flux absorbed in-depth
j	j th component	I_{ex}^0 ($W\ m^{-2}$)	Radiant heat flux through boundary
g	g th gaseous component	I_{rr} ($W\ m^{-2}$)	Radiant heat loss to environment
ξ_j ($kg\ m^{-3}$)	Mass concentration of j th component	N_g	Total number of gaseous components
t (s)	Time	E_i ($J\ mol^{-1}$)	Activation energy of i th reaction
N_r	Total number of reactions	R ($J\ mol^{-1}\ K^{-1}$)	Universal gas constant
θ_i	Stoichiometric mass coefficient of j th component in i th reaction	A_i	Arrhenius pre-exponential factor of i th reaction
r_i	Reaction rate of i th reaction	$COMP$	Reactant in given reaction
x (m)	Spatial coordinate	v_j	Volume fraction of j th component
J_j^x ($kg\ m^{-2}\ s^{-1}$)	Mass flux of j th component in x direction	k ($W\ m^{-1}\ K^{-1}$)	Thermal conductivity
ρ ($kg\ m^{-3}$)	Density	κ ($m^2\ kg^{-1}$)	Radiation absorption coefficient
N	Total number of components	σ ($W\ m^{-2}\ K^{-4}$)	Stefan–Boltzmann constant
C_p ($J\ kg^{-1}\ K^{-1}$)	Heat capacity	ε_j	Emissivity of j th component
T (K)	Temperature	λ ($m^2\ s^{-1}$)	Gas transfer coefficient
h_i ($J\ kg^{-1}$)	Heat of i th reaction	\dot{q}_x'' ($W\ m^{-2}$)	Conductive heat flux in x direction

The symbols used in these equations are defined in Table 1. The variables without subscripts denote the properties or state of component mixture.

Equation (1) is the mass conservation of the j th component that includes its consumption and production due to chemical reactions, diffusive/advective mass transport (if the component is a gas), and the mass transport associated with the expansion or contraction of the material. Equation (2) is the energy conservation that includes the heat generation or consumption due to chemical reactions or phase transitions, heat conduction, in-depth radiative heat transport, convective heat transfer associated with the movement of gases, and the heat flow due to expansion or contraction of the pyrolyzing material. Equations (3)–(7) further define the terms used in the conservation equations. It should be noted that, when first order, single-reactant reactions are defined within the modeling framework, as they were in the current study, the concentration of the second reactant ($COMP_2$) in equation (3) becomes equal to 1. A more detailed description of ThermaKin can be found in earlier publications.^{27,28}

The simultaneous thermal analysis (STA) and MCC samples were represented in the model as thermally thin and simulated using a single spatial element. The element temperature was forced to follow the experimental temperature profile by defining a sufficiently high convection coefficient, $1 \times 10^5\ W\ m^{-2}\ K^{-1}$, at the boundary. As shown in Figure 1, the sample heating rates observed in the experiments varied considerably before reaching the nominal (or set) values. To take these variations into account, the modeled heating rate was expressed via an exponentially decaying sinusoidal function of the form

$$\frac{dT}{dt}(t) = a_1 \{1 - \exp(-a_2 t) [\cos(a_3 t) + a_4 \sin(a_3 t)]\} \quad (8)$$

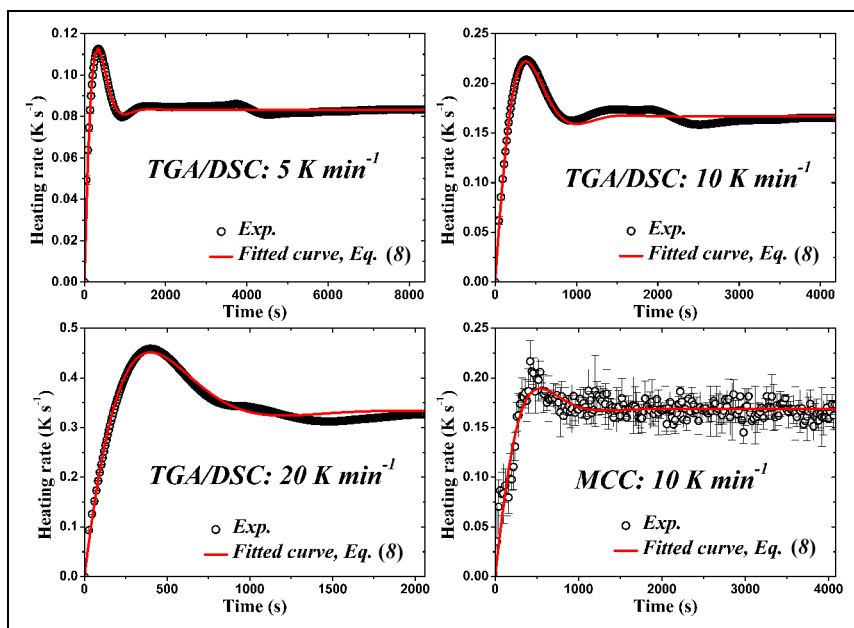


Figure 1. Averaged experimental and fitted heating rate profiles obtained for the TGA/DSC and MCC tests.

Table 2. Parameters describing evolution of instantaneous heating rate in the TGA/DSC and MCC tests.

Nominal heating rate	a_1 (K s^{-1})	a_2 (s^{-1})	a_3 (s^{-1})	a_4 (–)
5 K min^{-1} (TGA/DSC)	0.0834	0.00384	0.00484	–1.2338
10 K min^{-1} (TGA/DSC)	0.1670	0.00306	0.00510	–0.7544
20 K min^{-1} (TGA/DSC)	0.3245	0.00313	0.00354	–1.5110
10 K min^{-1} (MCC)	0.1686	0.00345	0.00405	–0.2617

TGA: thermogravimetric analysis; DSC: differential scanning calorimetry; MCC: microscale combustion calorimetry.

where a_1 (K s^{-1}), a_2 (s^{-1}), a_3 (s^{-1}), and a_4 are constants fitted to capture experimental data. The values of the constants are summarized in Table 2. The resulting fits are shown in Figure 1. All fitted curves have the coefficient of determination larger than 0.95. The mass flow boundary conditions were defined in the model such that the gaseous pyrolyzate instantaneously escaped the element.

A hill climbing (HC) optimization algorithm implemented as a MatLab script was coupled with ThermaKin to automate inverse analysis of the TGA data and determine the kinetic parameters of the OSB decomposition. A single goodness of fit criterion, GoF_M , was introduced to serve as a target of the optimization

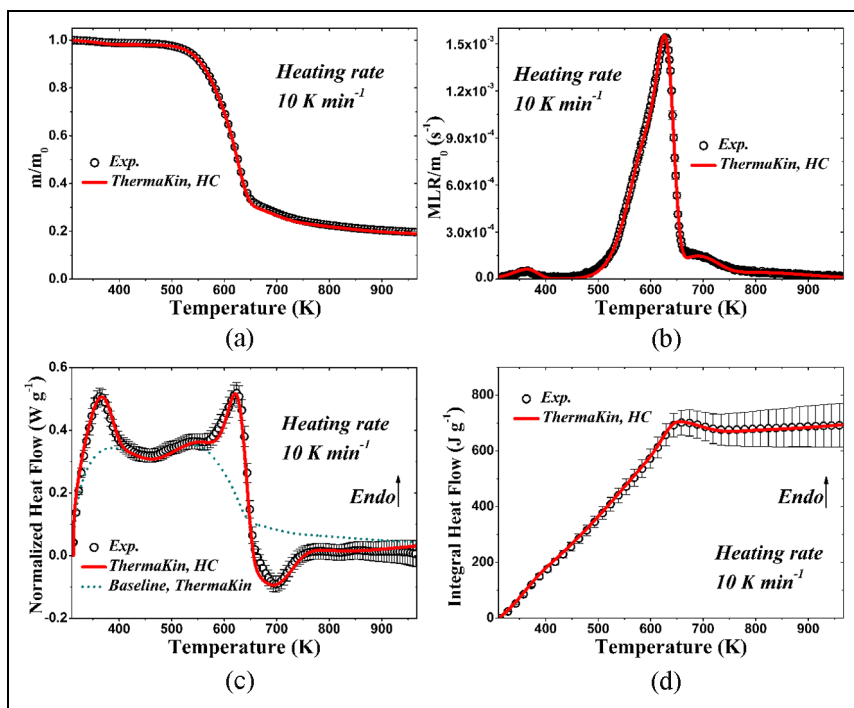


Figure 2. Experimental and simulated TGA ((a), (b)) and DSC ((c), (d)) data obtained for OSB at 10 K min^{-1} .

$$GoF_M = 1 - \left(\frac{0.6}{MLR_{max,exp}} \sqrt{\frac{\sum_i^N (MLR_{i,exp} - MLR_{i,model})^2}{N}} + \frac{0.4}{m_{max,exp}} \sqrt{\frac{\sum_i^N (m_{i,exp} - m_{i,model})^2}{N}} \right) \quad (9)$$

In equation (9), MLR is the mass loss rate and m is the sample mass. The subscripts max , exp , and $model$ denote the maximum, experimental, and modeled values, respectively. N is the total number of experimental data points. This criterion was formulated to obtain the best compromise between capturing both the MLR and mass profiles of a wide range of pyrolyzable solids. A GoF_M of 1 implies a perfect fit. More details on the algorithm implementation can be found in an earlier publication.²⁹

Results and discussion

TGA/DSC data analysis and model development

Figure 2 presents the mean mass (m), mass loss rate (MLR), heat flow, and integral of heat flow normalized by the initial mass (m_0) obtained in the experiments performed at 10 K min^{-1} . The uncertainties in the experimental data (shown as open circles) were calculated from the

Table 3. A reaction mechanism for the thermal decomposition of OSB (1.9 wt.% Water + 98.1 wt.% OSB component).

Reaction #	Reaction equation
1	Water \rightarrow Water_vapor
2	OSB \rightarrow 0.72 OSB_int1 + 0.28 OSB_gas1
3	OSB_int1 \rightarrow 0.45 OSB_int2 + 0.55 OSB_gas2
4	OSB_int2 \rightarrow 0.77 OSB_int3 + 0.23 OSB_gas3
5	OSB_int3 \rightarrow 0.77 Char + 0.23 OSB_gas4

OSB: oriented strand board.

scatter of the data as two standard deviations of the mean. The reproducibility of the TGA results is excellent throughout, while the scatter of the DSC data increases with increasing temperature due to reduction in the sample mass and increasing baseline uncertainties.

Five reactions can be identified from the MLR curve in Figure 2(b): the first peak located below 400 K, the asymmetric shoulder of the main peak, the main peak, the minor peak at about 700 K, and the slowly decaying segment above 750 K. The first peak can be attributed to vaporization of chemically bound water. This water, in the amount of 1.9 wt.%, is likely to be retained by OSB even under the driest environmental conditions and, therefore, its loss should be included in the thermal decomposition mechanism. The peaks associated with the second to fourth reactions can be identified from the MLR and heat flow curves to be located at 540, 625, and 700 K, respectively. These peaks can also be identified using the second derivative of thermogravimetry (DDTG) curve proposed by Li et al.⁴ to distinguish overlapping reactions. These and the last reaction can be attributed to the thermal decomposition of wood strands and adhesive.

As indicated by the experimental heat flow data in Figure 2(c), the first three reactions are either endothermic or thermally neutral but the fourth reaction is clearly exothermic. The presence of exothermic steps in the decomposition of charring polymeric solids was first observed and explained by Li and Stoliarov.¹⁴ Atreya et al.³⁰ found that wood particle pyrolysis consisted of an endothermic phase followed by an exothermic phase, which is consistent with the presented data.

In majority of earlier studies of engineered wood products,^{4,23} thermal decomposition models were formulated using a parallel reaction scheme. The assumption of parallel reactions is consistent with a multi-component nature of these lignocellulosic solids. However, this assumption also yields a requirement for the composition of the virgin material (initial concentration of individual components) to be specified. This composition is usually unknown and thus has to be obtained through optimization. Therefore, a decision was made to represent the thermal decomposition of OSB using a set of consecutive reactions, as shown in Table 3 (the stoichiometric coefficients reported in this table were obtained from optimization as discussed later in this section). The only parallel reaction that was used was the reaction that defined the loss of moisture. Using consecutive reactions allowed us to capture the experimental data with the minimum number of adjustable parameters and, thus, follow a widely adopted approach of the minimum complexity.

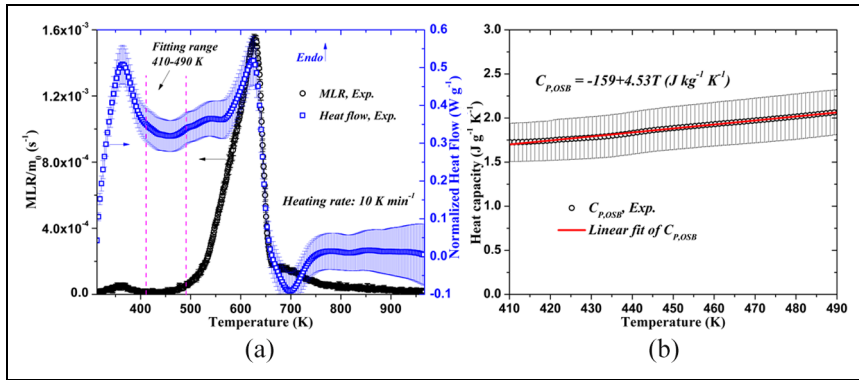


Figure 3. Determination of the heat capacity of undecomposed OSB: (a) Measured MLR and heat flow data; (b) linear fitting of heat capacity.

Table 4. Heat capacities of all condensed-phase components.

Component	C_p ($\text{J kg}^{-1} \text{K}^{-1}$)
Water	$5200 - 6.7T + 0.011T^2$
OSB	$-159 + 4.53T$
OSB_int1	$197 + 3.40T$
OSB_int2	$553 + 2.27T$
OSB_int3	$909 + 1.13T$
Char	1270

OSB: oriented strand board.

Heat capacity of the OSB component (representing undecomposed OSB) was obtained from the segment of DSC curve located between water vaporization and onset of decomposition, as shown in Figure 3(a), by dividing the measured heat flow by the instantaneous heating rate. The resulting heat capacity data were subsequently fitted with a linear function of temperature, as shown in Figure 3(b). The heat capacity of the final residue or char (represented by component Char in Table 3) was obtained in a similar manner. The heat capacity of water was obtained from the literature.³¹ The heat capacities of intermediate condensed-phase components could not be calculated directly and were assigned the values that interpolated between the heat capacities of the OSB and Char components in equal steps. All heat capacity data are summarized in Table 4.

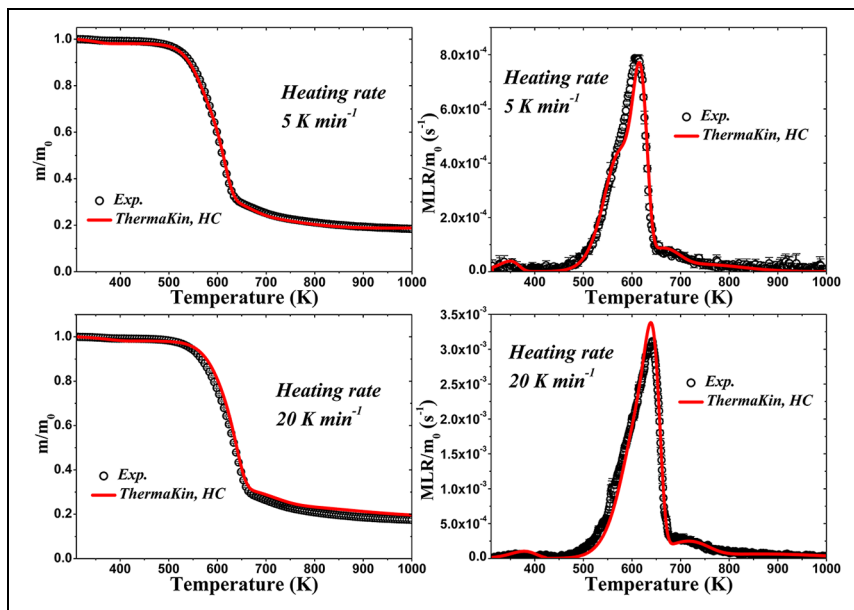
All reactions were assumed to be of the first order and their parameters (A , E , h , and stoichiometric coefficients) were optimized using HC algorithm to fit the experimental data at 10 K min^{-1} . The modeled curves shown in Figure 2 capture the TGA and DSC data well within the uncertainties of the measurements. The reaction parameters are given in Tables 3 and 5.

The heat of vaporization of water was optimized rather than taken from the literature because it was hypothesized to be affected by Van der Waals interactions between water molecules and wood components. Consistent with this hypothesis, the heat of vaporization was found to be about 20% higher in absolute value than that of pure water.³² Figure 2(c)

Table 5. Thermal decomposition reaction parameters obtained for OSB using the HC algorithm.

Reaction #	$A \text{ (s}^{-1}\text{)}$	$E \text{ (J mol}^{-1}\text{)}$	$h \text{ (J kg}^{-1}\text{)} \text{ (+ exo)}$
1	1.55×10^4	4.35×10^4	-2.78×10^6
2	1.56×10^7	1.04×10^5	-6.82×10^3
3	2.65×10^{12}	1.74×10^5	-1.37×10^5
4	8.93×10^3	8.37×10^4	2.90×10^5
5	4.40×10^{-1}	3.86×10^4	2.32×10^5

OSB: oriented strand board; HC: hill climbing.

**Figure 4.** Experimental and simulated TGA data obtained for OSB at 5 and 20 K min⁻¹.

shows the calculated sensible heat flow baseline, which helps delineate the endothermic (represented by reactions 2 and 3) and exothermic (represented by reactions 4 and 5) phases of the OSB decomposition. This baseline was computed by running the model with all heats of reaction set to 0. Excluding the contribution from water, the overall OSB decomposition process is essentially thermally neutral (the net heat of decomposition of $4.6 \times 10^4 \text{ J kg}^{-1}$).

Model validation and comparison with the models available in the literature

The ability of the model to make predictions at alternate heating rates is demonstrated in Figure 4. The predicted mass and MLR curves match the experimental results well, which intrinsically suggests that the presence of lids and/or changes in the crucible material had no

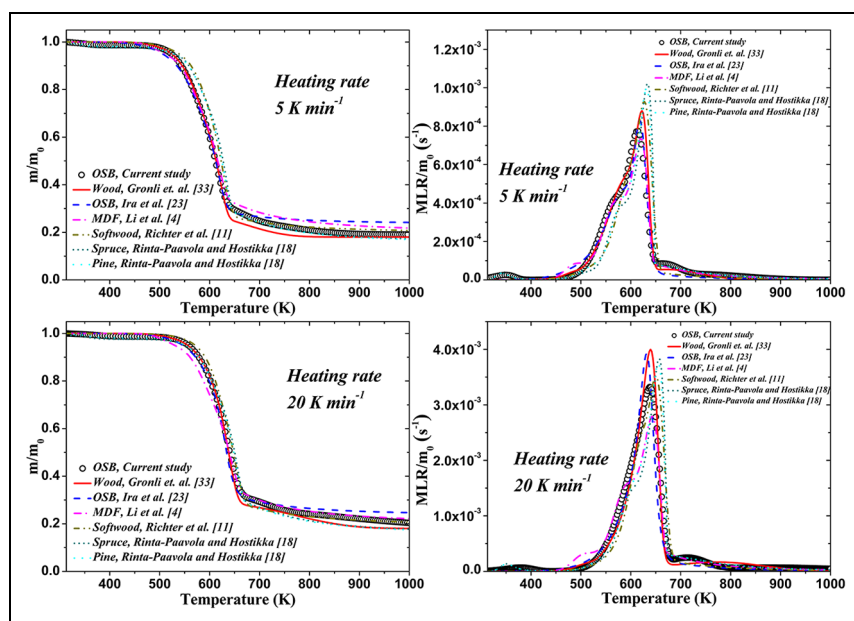


Figure 5. Comparison of mass and MLR data obtained for simulated idealized TGA conducted at 5 and 20 K min⁻¹ using the current and literature models for wood and engineered wood products.

impact on the decomposition kinetics. The model also accurately predicted the final residue yield obtained in the TGA experiments performed at a significantly higher heating rate. Two additional TGA tests were carried out at 50 K min⁻¹ in nitrogen to determine whether the residue yield displayed any significant dependence on heating rate. The residue yield did not show any heating rate dependence, which was accurately predicted by the model.

The OSB decomposition kinetics developed in this work was compared with several literature models obtained for wood,³³ OSB,²³ medium-density fiberboard (MDF),⁴ softwood,¹¹ and spruce and pine.¹⁸ Gronli et al.³³ collected the TGA data for four hardwoods and five softwoods and proposed a decomposition mechanism consisting of three parallel reactions: one for hemicellulose, one for cellulose, and one for lignin. A set of average kinetic parameters for the nine selected wood species was derived. Ira et al.²³ studied the pyrolysis of six engineered wood products, including an OSB, and also used a three-component parallel reaction scheme to model their measurements. Li et al.⁴ examined the thermal decomposition of MDF with additional consideration for resin (used as a binder), and utilized a four-component parallel reaction scheme. By compiling the pyrolysis data from the literature, Richter et al.¹¹ systematically investigated the effect of chemical composition on charring of softwood at both microscale and mesoscale using a three-component multiple-step reaction scheme. The average composition of softwood was determined to be 47, 24 and 29 wt.% of cellulose, hemicellulose, and lignin, respectively. Rinta-Paavola and Hostikka¹⁸ used a four-component parallel reaction mechanism to model TGA, DSC, and MCC data collected for spruce and pine.

Figure 5 shows the results of simulations of idealized TGA experiments performed at 5 and 20 K min⁻¹ heating rates using all these models, including the model developed in this

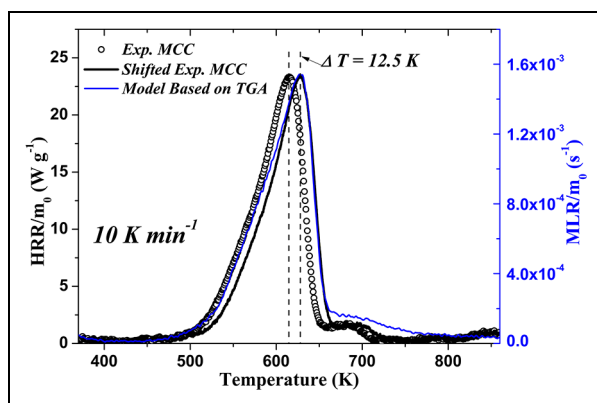


Figure 6. Comparison of unmodified and shifted average experimental HRR data with modeled MLR.

work. In these simulations, the heating rate was maintained perfectly constant throughout the heating process. Given a wide range of materials these models represent, the results are remarkably similar. Both the positions and shapes of the MLR peaks are very close and the final residue yields vary by only a few wt.%. This comparison suggests that, despite significant differences in the appearance and mechanical properties, the wood products used in the built environment have similar composition and the additives (including adhesives) are present in such low amounts that they do not significantly impact the overall thermal decomposition dynamics.

MCC data analysis

The heats of combustion, h_c , of the evolved gases defined in the OSB reaction mechanism were determined through modeling of the MCC data. First, the modeled MLR and experimental HRR were compared as shown in Figure 6. A slight mismatch between these signal profiles was identified and corrected by shifting the experimental MCC data by 12.5 K toward the higher temperature. This discrepancy was attributed to a non-uniformity in the temperature of the sample associated with additional heating of its top surface by radiation from the combustor, which was not fully captured by the MCC sample temperature sensor (located underneath the sample crucible).

During further analysis, MCC HRR data were generated from the modeling results by first assigning $1 \times 10^7 \text{ J kg}^{-1}$ heat of combustion value to all gases. Subsequently, these values were modified iteratively until the experimental average MCC data were matched by the model in accordance with a prescribed set of fitting criteria. These criteria were developed in earlier studies^{15,16} and comprised less than 5%, 5 K and 5% difference in the maximum HRR, temperature of the maximum, and final integral HRR value, respectively. It was determined that it was impossible to satisfy these criteria using a single value of the heat of combustion. Therefore, individual heats of combustion were assigned to individual gases. These heats of combustion are listed in Table 6. The predicted HRR and integral HRR are compared with the corresponding experimental results in Figure 7. The model shows nearly perfect agreement with the experiments. The net heat of combustion (the total heat released

Table 6. Heats of combustion of gaseous decomposition products.

Component	h_c (J kg ⁻¹)
Water_vapor	0
OSB_gas1	1.25×10^7
OSB_gas2	1.52×10^7
OSB_gas3	1.15×10^7
OSB_gas4	0.75×10^7

OSB: oriented strand board.

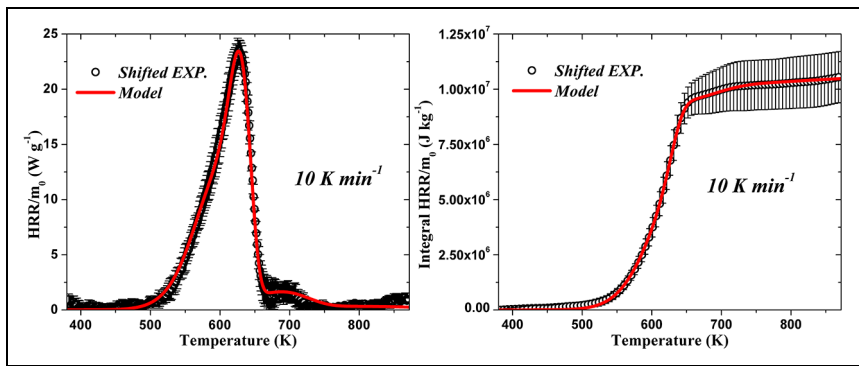


Figure 7. Comparison between the average experimental and simulated MCC data.

per unit mass gasified) predicted by the model, 1.31×10^7 J kg⁻¹, is close to the value 1.17×10^7 J kg⁻¹ measured for OSB in a cone calorimeter,²³ and to the values measured for spruce and pine, $\approx 1.4 \times 10^7$ J kg⁻¹, in an MCC.¹⁸

Conclusion

This study details a thermal decomposition model of OSB comprised of a water vaporization step and four consecutive, first-order reactions representing the decomposition of organic constituents of this material. Consecutive reactions were chosen over parallel reactions to capture the experimental data using the minimum number of adjustable parameters. This mechanism was developed using TGA and DSC experiments performed at a nominal heating rate of 10 K min⁻¹. The experiments were analyzed with a numerical model, ThermoKin, coupled with an HC optimization algorithm to determine the relevant kinetic and thermodynamic parameters. This parameter set was shown to accurately reproduce additional TGA data obtained at alternate heating rates of 5 and 20 K min⁻¹, which provided the necessary validation.

A series of MCC tests was also performed on this material. Modeling these tests yielded the heats of combustion of gaseous products of the decomposition reactions. These heats of combustion were found to vary between the reaction steps. Idealized TGA profiles at 5 and 20 K min⁻¹ obtained with the current model were compared with those generated using the

decomposition models of wood and engineered wood products available in the literature. All profiles were found to be remarkably similar indicating similarity in the chemical composition. Unfortunately, it was not possible to perform analogous comparisons of modeled DSC or MCC profiles due to the fact that the majority of the literature models lack the corresponding parameters. Part II of this work will focus on measuring relevant thermal and mass transport properties of OSB and validation of the complete pyrolysis model.

Acknowledgements

The authors would like to thank Dr Fernando Raffan-Montoya for help with the experiments and Dr Franz Richter of the University of California, Berkeley for insightful feedback.


Declaration of conflicting interests

The author(s) declared no potential conflicts of interest with respect to the research, authorship, and/or publication of this article.

Funding

The author(s) disclosed receipt of the following financial support for the research, authorship, and/or publication of this article: This work was supported by the U.S. National Institute of Standards and Technology (grant #70NANB19H053) and the National Natural Science Foundation of China (grant #51974164). The authors are grateful for this support.

ORCID iD

Junhui Gong  <https://orcid.org/0000-0003-0101-7448>

References

1. Marotte B. Toronto's Norbord riding the rising wave of OSB sales. *The Globe and Mail*, <https://www.theglobeandmail.com/report-on-business/forest-products-firm-norbord-riding-the-rising-wave-of-osb-sales/article30985989/> (accessed 20 September 2017).
2. Ferreira AI, Rabaçal M and Costa M. A combined genetic algorithm and least squares fitting procedure for the estimation of the kinetic parameters of the pyrolysis of agricultural residues. *Energy Convers Manag* 2016; 125: 290–300.
3. Abdelouahed L, Leveneur S, Vernieres-Hassimi L, et al. Comparative investigation for the determination of kinetic parameters for biomass pyrolysis by thermogravimetric analysis. *J Therm Anal Calorim* 2017; 128: 1201–1213.
4. Li K, Huang X, Fleischmann C, et al. Pyrolysis of medium-density fiberboard: optimized search for kinetics scheme and parameters via a genetic algorithm driven by Kissinger's method. *Energy Fuel* 2014; 28: 6130–6139.
5. Song C. Parameter estimation of the pyrolysis model for fir based on particle swarm algorithm. In: *Proceedings of the 2011 second international conference on mechanic automation and control engineering, Hohhot, China* 15–17 July 2011, pp. 2354–2357. New York: IEEE.
6. Xu L, Jiang Y and Wang L. Thermal decomposition of rape straw: pyrolysis modeling and kinetic study via particle swarm optimization. *Energy Convers Manag* 2017; 146: 124–133.
7. Ding Y, Zhang W, Yu L, et al. The accuracy and efficiency of GA and PSO optimization schemes on estimating reaction kinetic parameters of biomass pyrolysis. *Energy* 2019; 176: 582–588.
8. Richter F and Rein G. Pyrolysis kinetics and multi-objective inverse modelling of cellulose at the microscale. *Fire Safety J* 2017; 91: 191–199.
9. Richter F and Rein G. Heterogeneous kinetics of timber charring at the microscale. *J Anal Appl Pyrol* 2019; 138: 1–9.
10. Richter F and Rein G. Reduced chemical kinetics for microscale pyrolysis of softwood and hardwood. *Bioresour Technol* 2020; 301: 122619.
11. Richter F, Atreya A, Kotsovinos P, et al. The effect of chemical composition on the charring of wood across scales. *P Combust Inst* 2019; 37: 4053–4061.
12. Stoliarov SI, Saffronava N and Lyon RE. The effect of variation in polymer properties on the rate of burning. *Fire Mater* 2009; 33: 257–271.
13. Li J and Stoliarov SI. Measurement of kinetics and thermodynamics of the thermal degradation for non-charring polymers. *Combust Flame* 2013; 160: 1287–1297.
14. Li J and Stoliarov SI. Measurement of kinetics and thermodynamics of the thermal degradation for charring polymers. *Polym Degrad Stab* 2014; 106: 2–15.

15. McKinnon MB and Stoliarov SI. Pyrolysis model development for a multilayer floor covering. *Materials* 2018; 8: 6117–6153.
16. McKinnon MB, Ding Y, Stoliarov SI, et al. Pyrolysis model for a carbon fiber/epoxy structural aerospace composite. *J Fire Sci* 2017; 35: 36–61.
17. Ding Y, McKinnon MB, Stoliarov SI, et al. Determination of kinetics and thermodynamics of thermal decomposition for polymers containing reactive flame retardants: Application to poly(lactic acid) blended with melamine and ammonium polyphosphate. *Polym Degrad Stabil* 2016; 129: 347–362.
18. Rinta-Paavola A and Hostikka S. *A model for pyrolysis and oxidation of two common structural timbers*. Tallinn: Forum Wood Building Baltic, 2019.
19. Hirle S and Balog K. The effect of the heat flux on the self-ignition of oriented strand board. *J Slovak Univ Technol* 2017; 25: 123–129.
20. White RH and Sumathipala K. Cone calorimeter tests of wood composites. In: *Proceedings of the fire and materials 2013 conference*, San Francisco, CA, 28–30 January 2013, pp. 401–412. <https://www.fs.usda.gov/treesearch/pubs/44266>
21. Ayrlmis N, Candan Z and White R. Physical, mechanical, and fire properties of oriented strand board with fire retardant treated veneers. *Holz Roh Werkst* 2007; 65: 449–458.
22. Mealy C, Boehmer H, Scheffey JL, et al. *Characterization of the flammability and thermal decomposition properties of aircraft skin composite materials and combustible surrogates*. Federal Aviation Administration report no. DOT/FAA/TC-14/1, 1 March 2014, Atlantic City, NJ: Federal Aviation Administration.
23. Ira J, Hasalova L, Salek V, et al. Thermal analysis and cone calorimeter study of engineered wood with an emphasis on fire modelling. *Fire Technol* 2020; 56: 1099–1132.
24. Korobeinichev O, Gonchikzhapov M, Tereshchenko A, et al. An experimental study of horizontal flame spread over PMMA surface in still air. *Combust Flame* 2018; 188: 388–398.
25. ASTM Standard D7309: 2013. *Standard test method for determining flammability characteristics of plastics and other solid materials using microscale combustion calorimetry*. ASTM Int.
26. Lyon RE, Walters RN, Stoliarov SI, et al. Principles and practice of microscale combustion calorimetry. *Federal Aviation Administration report no. DOT/FAA/TC-12/53*, April 2013, Atlantic City, NJ: Federal Aviation Administration.
27. Stoliarov SI and Lyon RE. Thermo-kinetic model of burning for pyrolyzing materials. *Fire Safety Sci* 2008; 9: 1141–1152.
28. Stoliarov SI, Leventon IT and Lyon RE. Two-dimensional model of burning for pyrolyzable solids. *Fire Mater* 2014; 38: 391–408.
29. Fiola GJ, Chaudhari DM and Stoliarov SI. Comparison of pyrolysis properties of extruded and cast Poly (methyl methacrylate). *Fire Safety J*. In Press. 3 May 2020. <https://doi.org/10.1016/j.firesaf.2020.103083>
30. Atreya A, Olszewski P, Chen Y, et al. The effect of size, shape and pyrolysis conditions on the thermal decomposition of wood particles and firebrands. *Int J Heat Mass Tran* 2017; 107: 319–328.
31. McKinnon MB, Stoliarov SI and Witkowski A. Development of a pyrolysis model for corrugated cardboard. *Combust Flame* 2013; 160: 2595–2607.
32. Incropera FP, DeWitt DP, Bergman TL, et al. *Fundamentals of heat and mass transfer*. 6th ed. Hoboken, NJ: John Wiley & Sons, Inc, 2007.
33. Gronli MG, Varhegyi G and Blasi CD. Thermogravimetric analysis and devolatilization kinetics of wood. *Ind Eng Chem Res* 2002; 41: 4201–4208.